LUND UNIVERSITY

Revealing the mechanisms of hydrogel formation by laccase crosslinking and regeneration of feruloylated arabinoxylan from wheat bran

Yilmaz-Turan, Secil; Lopez-Sanchez, Patricia ; Jiménez-Quero, Amparo; Plivelic, Tomás S.; Vilaplana, Francisco

Revealing the mechanisms of hydrogel formation by laccase crosslinking and regeneration of feruloylated arabinoxylan from wheat bran

Secil Yilmaz-Turan [a,*], Patricia Lopez-Sanchez [b], Amparo Jiménez-Quero [a], Tomás S. Plivelic [c], Francisco Vilaplana [a,**]

[a] *Division of Glycoscience, Department of Chemistry, School of Engineering Sciences in Chemistry, Biotechnology and Health, KTH Royal Institute of Technology, AlbaNova University Centre, SE-106 91, Stockholm, Sweden*
[b] *Division of Food and Nutrition Science, Biology and Biological Engineering, Chalmers University of Technology, SE-412 96, Gothenburg, Sweden*
[c] *MAX IV Laboratory, Lund University, PO Box 118, 221 00, Lund, Sweden*

ARTICLE INFO

ABSTRACT

Feruloylated arabinoxylan (FAX) from cereal brans has large potential to generate multifunctional materials with customized macromolecular and nanostructural architectures and techno-functional properties. Here we investigate the chemical and structural mechanisms of hydrogel formation of wheat bran FAX following enzymatic crosslinking by laccase and a subsequent regeneration procedure involving freeze-drying and resuspension of the crosslinked FAX in different pH buffers, using a battery of biochemical, rheological and physical techniques. The laccase crosslinking induced the conversion of ferulic acid units into a wide diversity of dimeric forms, leading to an increased molecular weight and a closer-packing of the FAX chains. The regeneration step resulted in a remarkable increase in the viscosity and viscoelasticity for all tested pH values. The amount of crystallinity of FAX increased by enzymatic crosslinking, it was however decreased by the regeneration step. The structural characterization revealed that enzymatic crosslinking, in addition to the formation of covalent crosslinks, influences the physical intermolecular interactions between adjacent FAX domains, and the regeneration forms larger clusters with higher dynamic moduli. Our results reveal that both chemical and physical mechanisms influence the network formation and multiscale assembly of wheat bran FAX hydrogels, thus modulating their rheological properties fundamental for their use in food and biomedical applications.

1. Introduction

Wheat bran, the outer layers (epidermis, hypodermis, cross cells, tube cells, seedcoat, nucellar tissue, and aleurone) that surround the wheat endosperm, is the major by-product of flour production. As the human gastrointestinal system cannot fully digest its components, and due to the poor organoleptic properties, wheat bran is mainly used as an ingredient in animal feed (Prückler et al., 2014). Nonetheless, wheat bran is a rich source of polysaccharides such as arabinoxylans (AX) and phenolic compounds such as ferulic acid (FA), which can be used for novel material applications (Borjesson, Westman, Larsson, & Strom, 2019; Yilmaz-Turan, Jimenez-Quero, Menzel, et al., 2020). AX is a structural polysaccharide of the plant cell wall and constitutes a part of the dietary fiber portion of cereals, contributing to their functional properties and nutritional value (e.g. rheology in food products and prebiotic properties during gut fermentation) (Kaur et al., 2019; Rosicka-Kaczmarek, Komisarczyk, Nebesny, & Makowski, 2016). AX from wheat bran is constituted by $(1 \rightarrow 4)$-linked β-D-xylopyranose (Xyl*p*) units substituted by α-$(1 \rightarrow 2)$- and/or α-$(1 \rightarrow 3)$-linked L-arabinofuranosyl (Ara*f*). Wheat bran AX is esterified by FA (Fig. 1a) in the native cereal cell walls, which provides the bran with bioactive properties (Mendis & Simsek, 2014) and creates junction points for crosslinking. We have already demonstrated that feruloylated AX (FAX) can be isolated from cereal bran using subcritical water extraction, preserving the polymeric structure and the ester-linked FA substitutions (Ruthes, Martínez-Abad, Tan, Bulone, & Vilaplana, 2017; Yilmaz-Turan, Jimenez-Quero, Moriana, et al., 2020).

The oxidative coupling of FAX can be achieved using oxidative enzymes, i.e. laccase and peroxidase in the presence of O_2 and hydrogen peroxide (H_2O_2) as free radical-generating agents, respectively (Fig. 1b).

---

* Corresponding author.
** Corresponding author.
E-mail addresses: secilyt@kth.se (S. Yilmaz-Turan), franvila@kth.se (F. Vilaplana).

a) Wheat bran cell wall composition and structure of AX and crosslinked AX

Cereal bran

Molecular structure of F-AX in cereal bran
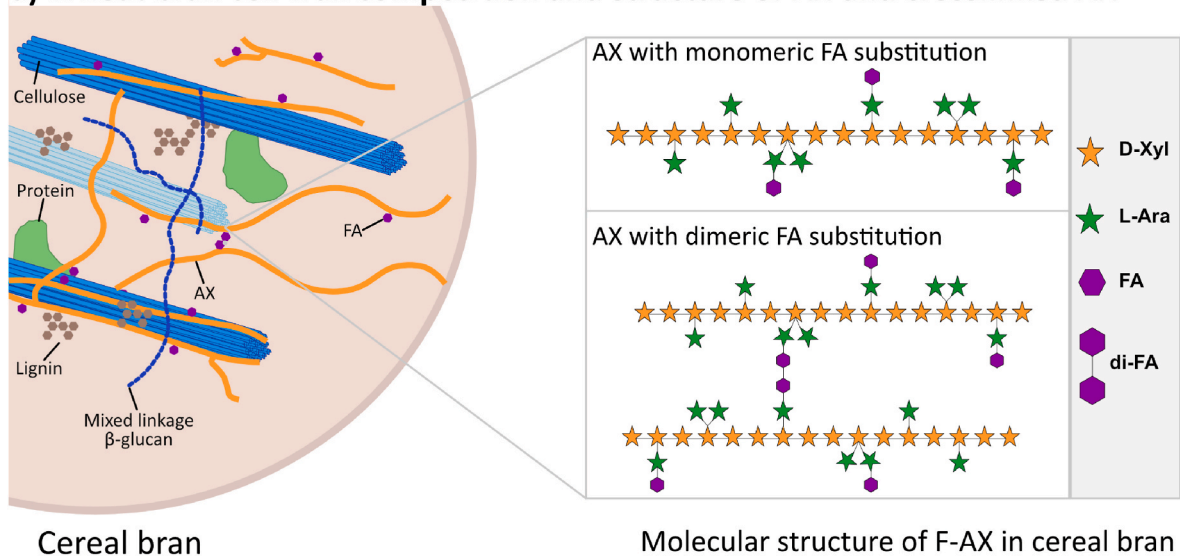
b) Structure of AX before and after laccase crosslinking

Native F-AX

Laccase
or
Peroxidase
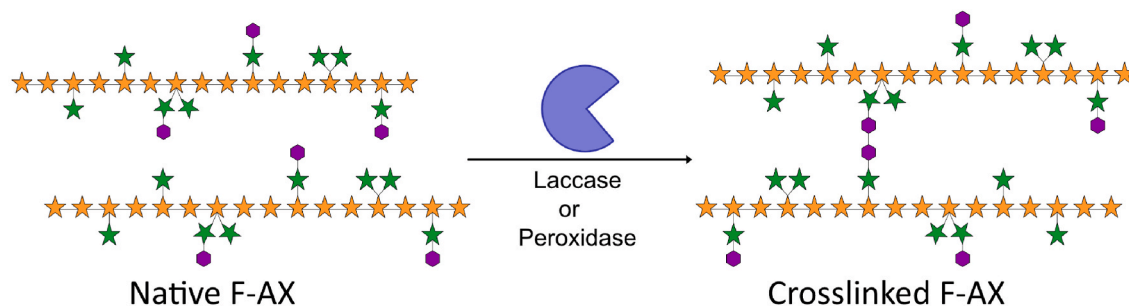
Crosslinked F-AX

c) Structure of di-FAs in crosslinked AX

8-8′ C di-FA

8-O-4′ di-FA

8-5′ C di-FA

8-8′ NC di-FA

5-5′ di-FA

8-5′ NC di-FA

Fig. 1. (a) Molecular structure of feruloylated wheat bran arabinoxylan. (b) Molecular structure of crosslinked arabinoxylan. (c) Structure of dehydrodimers of ferulic acid (di-FAs) in crosslinked arabinoxylan.

The dimerization of FA into its dehydrodimers (di-FAs) is enabled by its collision by a formed free radical, and the free radical chain reactions are terminated by the electron-donating groups on the benzene ring of the FA molecule (Mathew, Abraham, & Zakaria, 2015). The coupling of unpaired electrons of two different radicals leads to the formation of a covalent linkage between AX chains. During the enzymatic coupling reaction, monomeric FA is oxidized and converted into di-FAs, including 8–5′-cyclic, 8–5′-non-cyclic, 5-5′, 8-8′ and 8-O-4′ isomers (Fig. 1c). Some studies have also reported the formation of dehydrotrimer forms of FA such as the 4-O-8'/5'-5″ isomer (Carvajal-Millan, Landillon, et al., 2005).

The enzymatic cross-linking of FAX chains yields a three-dimensional network, in which the water phase is retained and a hydrogel is formed. The main force that drives the gelation of FAX and governs the gel properties is the formation of covalent linkages between the polymeric chains. On the other hand, non-covalent interactions suc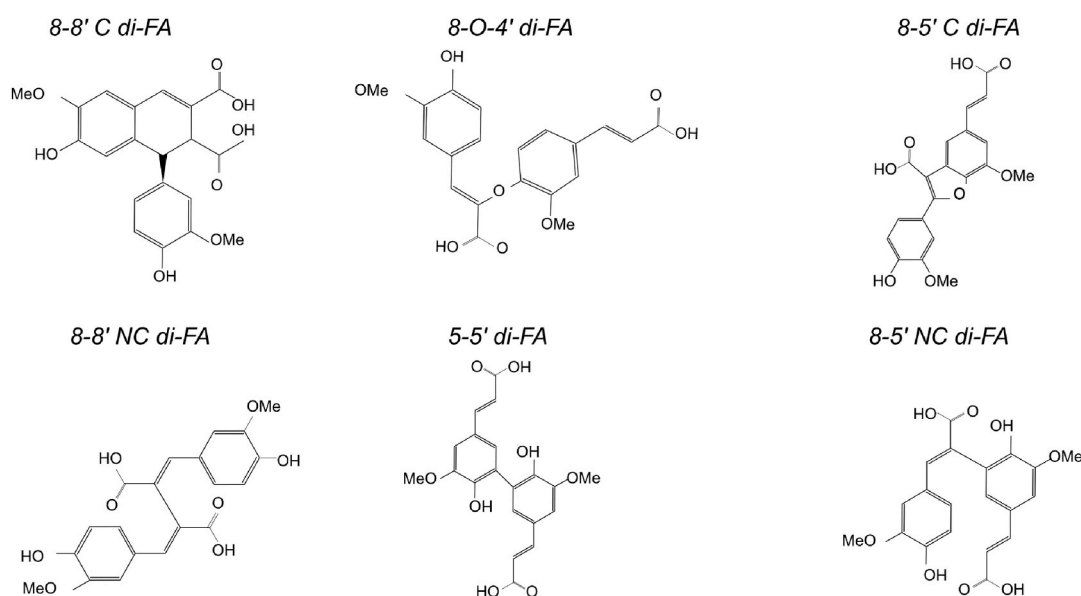h as hydrogen bonding have been considered to contribute to the stability of such hydrogels (Vansteenkiste, Babot, Rouau, & Micard, 2004). The degree of covalent and non-covalent interactions between FAX chains depends on the molecular properties of the source AX, including the degree of substitution (DS), degree of feruloylation and molecular weight, and will influence the physicochemical properties of the resulting hydrogel. For example, Carvajal-Millan, Landillon, et al. (2005) have shown that the storage modulus of AX hydrogels increases as the FA content increases. Marquez-Escalante et al. (2018) have reported that lower DS of AX improves the mechanical strength of AX hydrogels and enhances the covalent bonding between AX chains. Despite the understanding of the effect of the molecular structure of AX on the hydrogel properties, the conformational changes occurring upon covalent cross-linking and the nature of supramolecular interactions and the multiscale assembly within the FAX network remain unclear. Recently, Zhang, et al. (2019) reported the formation of stronger FAX hydrogels in acidic conditions, which was attributed to hydrogen bonding between FAX chains, particularly with low Araf substitution. For low branched AX, the overall mechanism resulting in network formation may be hidden behind their short-range order, i.e. crystallinity. Several studies have analyzed the crystal structure of AX from different cereal sources in their solid state (film) and demonstrated that films from low-DS AX can reach up to 20% degree of crystallinity (X_c) (Heikkinen et al., 2013; Hoije, Sternemalm, Heikkinen, Tenkanen, & Gatenholm, 2008; Stevanic et al., 2011; Zhang et al., 2011). However, the existence of crystalline domains in AX hydrogels has not been reported yet, which represent a completely different state of AX (i.e. hydrated). Furthermore, little is known about the assembly of enzymatically-crosslinked FAX hydrogels on the nanometric length scale. In this direction, small angle X-ray scattering (SAXS) has been used to understand the network formation and structure of polysaccharide gels from different plant sources (Schuster, Cucheval, Lundin, & Williams, 2011; Yu et al., 2019), thus complementing the information obtained from rheological and microscopic characterization.

In this study, we aim to elucidate the multiscale assembly mechanisms that drive the gelation of FAX hydrogels by enzymatic crosslinking and regeneration in various pH conditions combining complementary biochemical and biophysical characterization tools. Firstly, we have monitored the amount and diversity of covalent diferulic bridges and the molar mass changes upon enzymatic crosslinking of FAX. Secondly, the FAX hydrogels were regenerated in varying pH conditions and the rheological properties were characterized. Cryogenic scanning electron microscopy (Cryo-SEM), wide angle and small angle X-ray scattering (WAXS and SAXS) techniques were used to study the structural properties of the hydrogels at different length scales. Finally, the integration of this structural information has allowed us to propose a model for the assembly of FAX hydrogels with low DS upon enzymatic gelation and regeneration, which explains the range of rheological properties obtained and provides the basis for further potential applications.

2. Material and methods

2.1. Materials

Wheat bran was kindly provided by Lantmännen (Stockholm, Sweden) with the composition presented in Supplementary Table S1 (Yilmaz-Turan, Jimenez-Quero, Moriana, et al., 2020). All chemicals, reagents and enzymes were purchased from Sigma-Aldrich (Stockholm, Sweden) unless stated otherwise. The 5-5′ and 8–8′ ferulic acid dehydrodimers were kindly donated by Prof. Florent Allais and Amandine Léa Flourat (AgroParisTech, Pomacle, France).

2.2. Preparation of the hydrogels by enzymatic crosslinking and regeneration

Feruloylated arabinoxylan was extracted from wheat bran by subcritical water extraction as described in our previous study (Yilmaz-Turan, Jimenez-Quero, Menzel, et al., 2020), named as FAX and used for the crosslinking. The composition of FAX is presented in Supplementary Table 1. The crosslinking of FAX was carried out using laccase from *Trametes versicolor* (EC 1.10.3.2). FAX was solubilized in water (5% w/v) and laccase was added to the solution at a dosage of 1.675 nkat/mg AX. The reaction was kept at 30 °C under constant stirring for 24 h and this sample was named FAX-CL. To monitor the gelation of FAX at different pH, FAX-CL was freeze-dried and then resuspended in hydrogels citrate phosphate buffer at pH 2.0, 5.0 and 7.0 to regenerate hydrogels from FAX-CL (5% w/v). The regenerated hydrogels were named FAX-CL-pH2, FAX-CL-pH5 and FAX-CL-pH7, respectively.

2.3. Methods of analysis

2.3.1. Molecular weight distribution

The molecular weight distributions of FAX and FAX-CL were analyzed using size exclusion chromatography (SECcurity 1260, Polymer Standard Services, Mainz, Germany) coupled to a multi-angle laser light scattering (MALLS) detector (BIC-MwA7000, Brookhaven Instrument Corp., US) and a refractive index detector (SECcurity 1260, Polymer Standard Services, Mainz, Germany) thermostated at 45 °C. The samples were dissolved in dimethyl sulfoxide (DMSO) with 0.5% w/v lithium bromide (LiBr) at a concentration of 3 mg/mL to achieve molecular dissolution of the cross-liked FAX chains and avoid aggregation artifacts. SEC analyses were performed using GRAM 30 and 10 000 analytical columns (PSS, Mainz, Germany) and DMSO-LiBr as the mobile phase at a flow rate of 0.5 mL min^{-1}. The calibration of the size distributions was carried out using pullulan standards (PSS, Mainz, Germany) with a molecular weight range of 342–708 000 Da. The conversion of elution volumes (V_{el}) into hydrodynamic volumes (V_h) was performed by universal calibration using the Mark-Houwink equation for pullulan standards (Vilaplana & Gilbert, 2010). The Mark-Houwink parameters for pullulan in DMSO-LiBr are K = 2.427 × 10^{-4} dL g^{-1} and a = 0.6804 (Kramer and Kilz, PSS, Mainz, Germany, private communication). The data are presented in terms of hydrodynamic radius (R_h), corresponding to the equivalent of hydrodynamic volume (V_h) by the equation of $V_h = 4/3\pi R_h^3$. The absolute weight-average molecular weight as a function of hydrodynamic size, $M_w(V_h)$, was derived from the MALLS detector at each slice of elution volume using Zimm extrapolation, using a refractive index increment (dn/dc) of 0.0853 mL g^{-1} for polysaccharides in DMSO/LiBr 0.5% w/w (Vilaplana et al., 2010).

2.3.2. Quantification of phenolic acid content

The phenolic acid content of all samples (in triplicates) was determined after saponification by 2 M NaOH (20:1, w/v) at 30 °C overnight, subsequent acidification by 37% HCl and extraction with ethyl acetate (2:1 v/v). The extracted samples were dried under nitrogen flow and resuspended in methanol:2% acetic acid mixture (1:1 v/v) and analyzed

by an HPLC system (Waters 2695 separation module, Waters 2996 photodiode array detector; USA) coupled to a UV/Vis detector, equipped with a C18 guard column and an SB-C18 separation column (Zorbax SB-C18 5 μm particle size, 4.6 × 250 mm, Agilent, USA). The separation was performed at 25 °C and 1 mL min⁻¹ flow rate using a gradient of 2% acetic acid and absolute methanol, as described by Menzel, Gonzalez-Martinez, Chiralt, and Vilaplana (2019). A standard calibration was recorded at 270 nm and 325 nm using caffeic acid, *p*-coumaric acid, ferulic acid, cinnamic acid, 5-5′ di-FA and 8-8′ di-FA at concentrations between 0.005 g/L and 0.1 g/L.

2.3.3. Identification of ferulic acid dehydrodimers

The identification of the di-FAs was performed after saponification as described above using an HPLC system coupled to an electrospray ionization mass spectrometry (ESI-MS) using a Synapt G2 mass spectrometer (Waters, Milford, MA, USA). Capillary and cone voltages were 3 kV and 10 kV, respectively. Saponified samples of FAX and FAX-CL were suspended in 50% acetonitrile containing formic acid (0.1% v/v) and injected onto an Eclipse Plus C18 column (Agilent Technologies, Santa Clara, CA, USA). The mobile phase consisted of 0.1% (v/v) formic acid in water (Eluent A) and 0.1% (v/v) formic acid in acetonitrile (Eluent B). The eluent program was as follows: 95% A (2 min), 62% A (15 min), 10% A (3 min), 10% A (1 min), 95% A (5 min) and 95% A (1 min). A standard mixture of monomeric ferulic acid, 5-5′ di-FA and 8-8′ di-FA (0.1 mg/mL) was used to reference the retention time of the di-FAs in the samples. MS² analysis was carried out in positive mode with ion collision-induced dissociation (CID) using nitrogen as the collision gas. 369.1 m/z ion was selected for the fragmentation of the di-FAs and subjected to a collision energy of 20 eV. The chromatograms and spectra were analyzed using the MassLynx software (Waters, Milford, MA, USA).

2.3.4. Rheological characterization

The rheological tests were performed in duplicates using a strain-controlled rheometer (ARES G2, TA Instruments, New Castle, DE, USA) at 25 °C with a 20.0 mm parallel plate. Steady state shear viscosity measurements were carried out using a gap of 0.5 mm in a shear rate range from 1 to 10 s⁻¹. Viscoelastic properties were measured by small amplitude oscillatory shear using a frequency sweep test in a range of angular frequency of 0.6–125 rad s⁻¹ and a 0.5% oscillation strain, based on preliminary experiments to determine the linear viscoelastic region. A solvent trap was used to prevent drying of the samples.

2.3.5. Cryogenic scanning electron microscopy (Cryo-SEM)

The microstructure of the hydrogels was analyzed by cryo-SEM after high-pressure freezing (HPF) of the samples. Hydrogel samples were carefully scooped and loaded onto 6 mm aluminum sample platelets and frozen at high pressure using an HPM100 system (Leica Microsystems, Wetzlar, Germany). The frozen samples were stored in liquid nitrogen until analysis. Before cryo-SEM imaging, the frozen samples were sublimated under vacuum at −90 °C for 30 min and then coated with platinum for 10 s. The surface morphology was analyzed using a field emission scanning electron microscopy (FE-SEM) (Merlin, Carl Zeiss GmbH, Germany) fitted with a PP3000T cryo-SEM preparation system (Quorum Technologies, UK). Cryo-SEM images were taken at −140 °C using an in-chamber secondary electron detector (ETD) at an acceleration voltage of 3 kV and probe current of 50 pA. The cryo-SEM images were further analyzed using the open-source CellProfiler™ software to determine the porosity of the hydrogels. The porosity of the hydrogels was calculated by taking the ratio of the area of pores to the total area of images and expressed as a percentage.

2.3.6. Wide-angle (WAXS) and small-angle (SAXS) X-ray scattering

WAXS and SAXS measurements of FAX solution, FAX-CL and FAX-CL-pH2 were performed using the Mat:Nordic SAXS setup at the Chalmers Materials Analysis Laboratory at Chalmers University of Technology, Sweden. The main wavelength used was λ = 1.54 Å (0.154

nm) and the detection system was Pilatus 300K detector (Dectris, USA). For the WAXS and SAXS measurements, the FAX solution was placed in sealed quartz capillaries (2 mm diameter, 0.01 mm wall thickness) (Hilgenberg Gmbh, Germany) and the gels (FAX-CL and FAX-CL-pH2) were enclosed in sandwich cell holders with the entire volume constrained by a Kalrez O-ring (5.28 mm inner diameter, 1.78 mm thickness) and two mica windows of 15 μm thickness, respectively. The measurements were performed under vacuum. The scattering from a quartz capillary filled with water or with citrate phosphate buffer, or a sandwich cell holder filled with citrate phosphate buffer were subtracted from the measurements of the different samples. Silver behenate standard was used for the calibration of the angular range of the detection.

Moving the detector position with respect to the sample, WAXS and SAXS measurements were performed at 134 mm and 1084 mm, respectively. The q-range achieved was $0.007 \leq q \leq 0.25$ Å⁻¹, ($0.0007 \leq q \leq 0.025$ nm⁻¹) where $q = \frac{4\Pi}{\lambda} sin\theta$ and 2θ is the scattering angle. The exposure time of all the measurements was 600 s.

Basic data reduction operations were performed using the SAXSGUI software (Rigaku Innovative Technologies & JJ-XRay-Sytems-ApS, 2010). WAXS data was fitted using Origin® 9.0 2021 and the calculation of the lattice parameters, *a, b* and *c* for unit cells is described in the Supplementary Material. Modelling of the SAXS data was performed using the SasView 4.2.2 package (SasView).

2.3.7. Statistical analysis

The statistical analysis of the viscosity and WAXS analyses was done by a simple *t*-test. Differences were considered statistically significant when p was <0.05.

3. Results and discussion

3.1. Efficiency of laccase crosslinking and identification of ferulic acid dimers

In previous studies we have demonstrated that wheat bran FAX extracted by subcritical water extraction contains monomeric FA and its dehydrodimers (di-FAs) covalently attached to the AX chains (Ruthes et al., 2020). Here we aim to use these phenolic moieties as molecular handles for the covalent crosslinking of FAX chains by laccase oxidation for hydrogel formation. We monitored the biochemical efficiency of laccase crosslinking following the occurrence of monomeric FA and di-FAs by HPLC-ESI-MS² of both FAX and FAX-CL. HPLC-ESI-MS² analysis showed the presence of 6 different dimers in FAX and FAX-CL (Fig. 2a and b) with different peak intensities. The mass to charge ratios of these peaks were 369.1 m/z, corresponding to di-FAs in adduct with a proton [M − H₂O + H⁺]. To further identify the di-FAs, the 369.1 m/z ion was subjected to CID-MS² and the resulting spectra were assigned to corresponding di-FAs according to Vismeh et al. (2013). The 6 di-FA peaks corresponded to 8-8′ cyclic (C) (Figs. 2c), 8-8′ noncyclic (NC) (Figs. 2d), 5-5' (1) (Ac–Am) (Figs. 2e), 5-5' (2) (Di-Am) (Supplementary Fig. S2a), 8-O-4' (Fig. 2f) and presumably 8–5' di-FA (Supplementary Fig. S2b). The peak intensities of the di-FAs in FAX and FAX-CL were qualitatively compared to assess the efficiency of the enzymatic crosslinking. The most distinct increase in the intensities was observed in the 8-8′ NC di-FA peak (10.16 min), which also eluted at 11.59 min and increased upon enzymatic crosslinking (Fig. 2b). Similarly, the intensity of the 5-5′ di-FA (2) (Di-Am) (12.95 min) and the presumed 8–5′ di-FA (13.72 min) peaks increased but to a lesser extent. Interestingly, the peak intensity of 5-5′ Ac–Am di-FA (1) decreased after crosslinking, suggesting that it was converted to another di-FA, likely 5-5′ di-FA (2) (Di-Am).

In order to verify the changes observed by the HPLC-ESI-MS² analysis, the phenolic acid content of FAX and FAX-CL was determined by HPLC. In the FAX, FA was determined as the main phenolic acid together with a minor content of *p*-coumaric acid, 8-8′ di-FA and 5-5′ di-FA
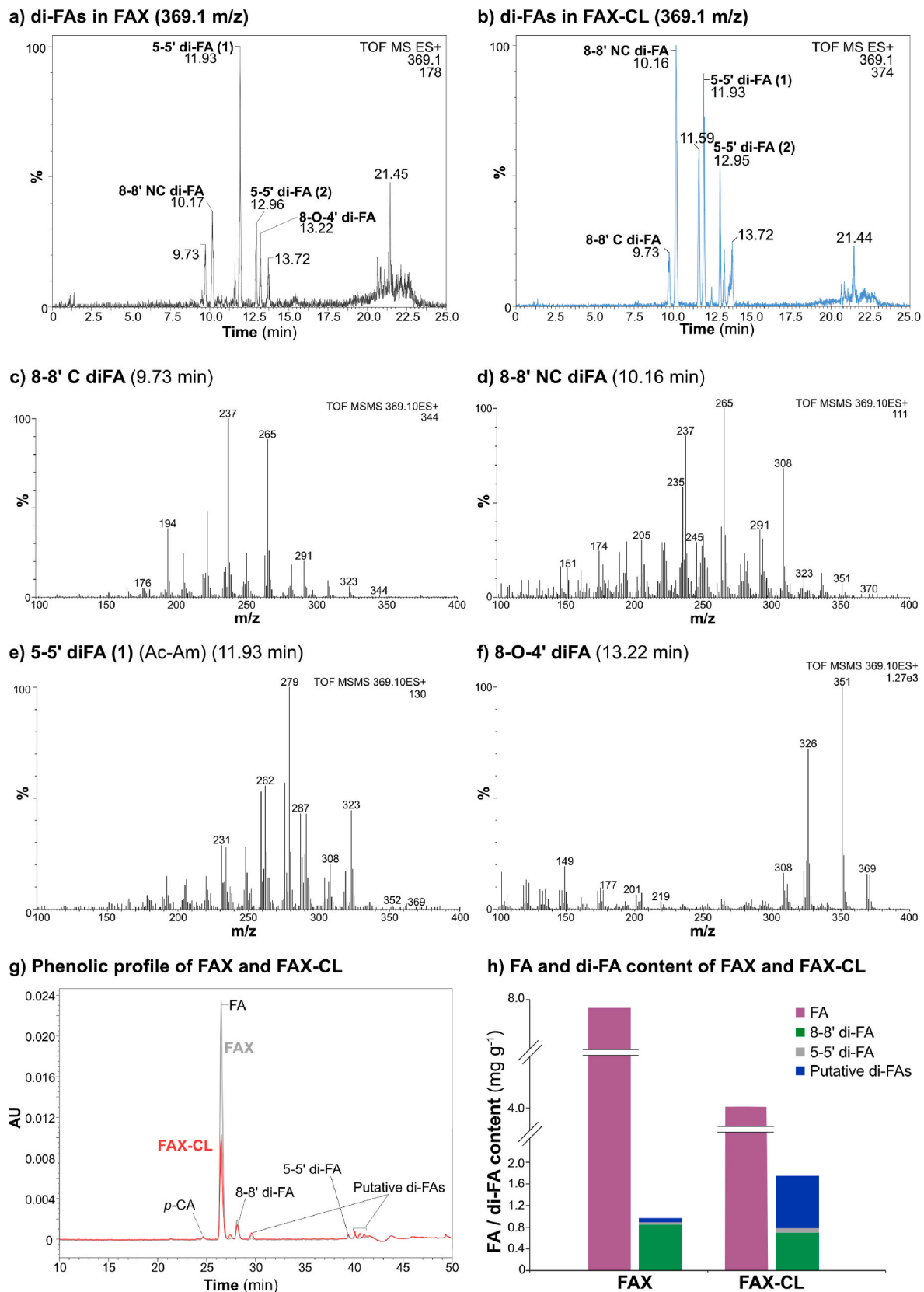
Fig. 2. Phenolic acid profiles of native and crosslinked wheat bran arabinoxylan. Ion extracted HPLC-ESI-MS chromatogram of (a) FAX, and (b) FAX-CL. (c–f) CID-MS^2 spectra of identified di-FA isomers. (g) HPLC chromatograms of FAX and FAX-CL. (h) Changes in the FA and di-FA content of FAX and FAX-CL.

(Fig. 2h). In the HPLC chromatogram of FAX (Fig. 2g), we observed small peaks eluting after the 8-8′ and 5-5′ di-FAs, which were attributed to the 8-O-4′ di-FA and 8–5′ di-FAs as the presence of these di-FAs was confirmed by the HPLC-ESI-MS^2 analysis (Fig. 2g). These two peaks were roughly quantified using the response factors of the 8-8′ and 5-5′ di-FAs, respectively, and combined as putative di-FAs (Fig. 2h and Supplementary Table S2). During enzymatic crosslinking, monomeric FA was depleted by 45% as it was converted to di-FAs. The change in the concentration of the 8-8′ and 5-5′ di-FAs was not pronounced in FAX-CL; however, the peaks of the putative di-FAs intensified (Fig. 2b). Indeed, the increase in the estimated amount of the putative di-FAs was approximately 12-fold (Fig. 2h and Supplementary Table S2). Furthermore, the relative decrease in the concentration of monomeric FA corresponded to the total increase in the amount of the di-FAs (45%), indicating that laccase oxidation of FA directly resulted in the formation of diferuloyl bridges.

Previous studies have reported different predominant di-FAs in crosslinked FAX from various cereal sources. For example, Khalighi, Berger, and Ersoy (2019) has determined the predominant dehydrodimer of FA in laccase-crosslinked wheat bran AX as 8-O-4' di-FA. On the other hand, 8-8′ di-FA and 8–5′ di-FA have been found as the main di-FAs in crosslinked corn bran AX by Zhang et al. (2019) and Martinez-Lopez et al. (2019), respectively. The dimerization of FA starts with the attack of the oxidizing agent (O_2) on the H atom of the hydroxyl group of FA, resulting in the formation of an unpaired electron (i.e. a phenoxy radical). In the presence of sufficient concentration of the oxidizing agent, numerous FA moieties are attacked, resulting in many phenoxy radicals. The position of the phenoxy radical varies due to their great number and the structure of the formed di-FAs merely depends on the position of the radicals. Therefore, di-FAs formed in our study were expected to be different from those previously reported as the formation of di-FAs is randomly induced by the coupling of the free radicals.

3.2. Enzymatic crosslinking influences the macromolecular architecture and conformation of FAX

The molar mass distributions and macromolecular conformation of the crosslinked AX (FAX-CL) was determined using multi-detection SEC and compared to that of the native FAX. The SEC weight distribution, w (logV$_h$), and the size dependence of the weight-average molecular weight, $\overline{M}_w(V_h)$, were presented as a function of the hydrodynamic radius (R$_h$) (Fig. 3a). The number-average molecular weight, $\overline{M}_n$, and weight-average molecular weight, $\overline{M}_w$ and dispersity (Đ) values of FAX and FAX-CL obtained by absolute calibration (light scattering) are represented in Table 1.

The use of DMSO-LiBr as a solvent and mobile phase of the SEC-MALLS ensures the molecular dissolution of the FAX and FAX-CL macromolecules, minimizing the occurrence of supramolecular interactions and aggregation between polymeric chains and without altering the covalent nature of the ferulic acid crosslinks. FAX showed a monomodal molar mass distribution and the average molar mass was similar to that reported in our previous study (Yilmaz-Turan, Jimenez-Quero, Menzel, et al., 2020). Comparing the molar mass distribution of FAX-CL, we observe a shift of the w(log V$_h$) distribution to lower hydrodynamic radii (R$_h$) for the crosslinked FAX-CL sample compared to the original FAX. At the same time, the absolute molar mass at a certain hydrodynamic size, $\overline{M}_w(V_h)$ for FAX-CL was higher than FAX, strongly suggesting structural differences between these two AX. These two effects together indicate the covalent crosslinking of two or more FAX chains in FAX-CL (hence the increase in absolute molar mass for a specific hydrodynamic size), resulting in overall macromolecular structures with more compact hydrodynamic conformations (lower hydrodynamic sizes).
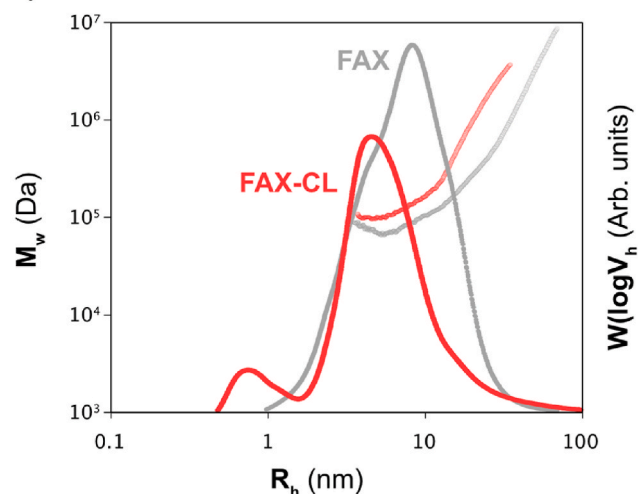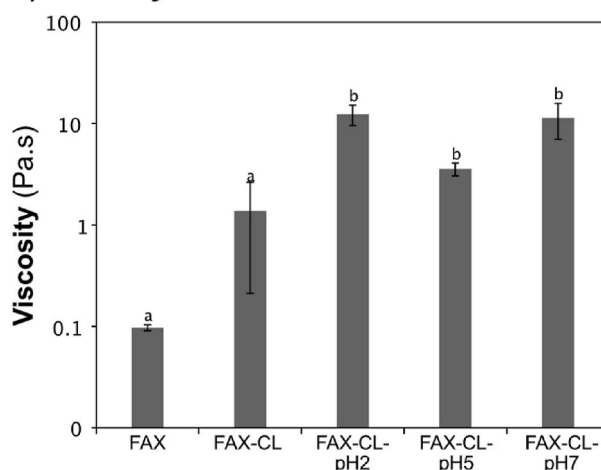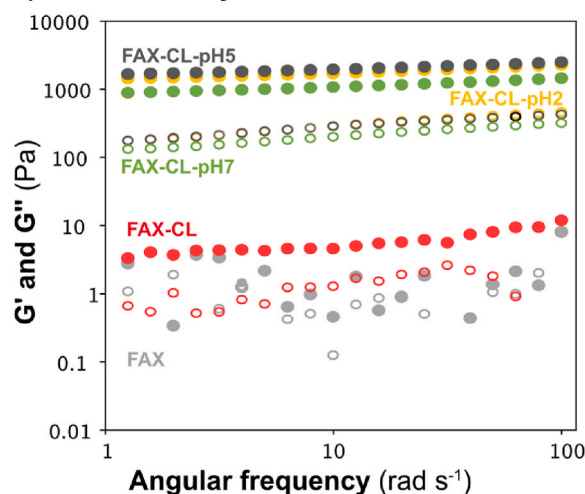
Fig. 3. Size distributions and rheology of native and crosslinked wheat bran arabinoxylan. (a) SEC size distribution of FAX and FAX-CL, (b) Apparent viscosity of FAX, FAX-CL, FAX-CL-pH2, FAX-CL-pH5 and FAX-CL-pH7 (all samples at 5%) at shear rate of 10 s^{-1}, (c) Storage modulus (G′) (full symbols) and loss modulus (G″) (open symbols) of FAX, FAX-CL, FAX-CL-pH2, FAX-CL-pH5 and FAX-CL-pH7. *Superscript letters in* Fig. 3b: *t-test of 2 replicates (p < 0.05). The G″ curves of FAX-CL-pH2 and FAX-CL-pH5 overlap.*

Table 1
Relative number-average (M_n) and weight-average (M_w) molecular weight, and polydispersity (D) of native (FAX) and crosslinked (FAX-CL) arabinoxylan using light scattering calibration.

	$\overline{M}_n$ (Da)	$\overline{M}_w$ (Da)	D
FAX	9.71×10^4	1.28×10^5	1.32
FAX-CL	1.43×10^5	1.59×10^5	1.11

3.3. Enzymatic crosslinking and regeneration fine-tune the strength of FAX hydrogels

To confirm the gelation of FAX-CL in water and to understand the gelation behavior of its regenerated counterparts at different pH values (FAX-CL-pH2, FAX-CL-pH5 and FAX-CL-pH7) shear viscosity and viscoelasticity measurements were performed (Fig. 3b and c). The apparent viscosity of the samples is presented at the shear rate of 10 s^{-1} (Fig. 3b) as no reliable data was obtained below 10 s^{-1} and all the samples displayed shear thinning behavior (Supplementary Fig. S3). The FAX solution exhibited the lowest apparent viscosity at 10 s^{-1} (0.10 ± 0.01 Pa s) and enzymatic crosslinking (FAX-CL) increased the apparent viscosity by approximately one order of magnitude (1.38 ± 1.10 Pa s) however, this difference was not statistically significant. This suggested that crosslinking of wheat bran AX by laccase results in the formation of covalently-bound polysaccharide networks with medium viscosity. Importantly, when regenerated in citrate phosphate buffer after freeze drying, the FAX gels had significantly higher viscosity compared to FAX-CL, increasing by almost 100-fold (12.34 ± 2.80 Pa s for FAX-CL-pH2). On the other hand, the pH conditions of the regeneration step did not substantially influence the viscosity values.

The dynamic storage (G′) and loss (G″) moduli were monitored by frequency sweep tests and are shown in Fig. 3c. FAX exhibited typical solution behavior at the measured concentration, whereas FAX-CL showed gel characteristics with G′ > G″ and higher moduli values than FAX. Regenerated hydrogels (FAX-CL-pH2, FAX-CL-pH5 and FAX-CL-pH7) had significantly higher moduli values where G′ was larger than G″; however, the pH of the buffer did not change the viscoelasticity. Viscoelasticity measurements revealed that FAX-CL-pH2, FAX-CL-pH5 and FAX-CL-pH7 were strong gels whereas FAX-CL displayed weak gel behavior. The change in the viscoelasticity behavior after enzymatic crosslinking (FAX-CL) confirmed the successful hydrogel formation, while the regeneration of FAX-CL after freeze-drying had more interesting implications. In a previous study, an increase in G′ and G″ of corn bran AX hydrogels has been reported, when regenerated at pH 2.0 but not at higher pH conditions (Zhang et al., 2019). The authors ascribed this rheological behavior at pH 2.0 to the neutralization of the carboxylic acid groups (of GlcA present in corn AX), which decreased the repulsive electrostatic forces between the polysaccharide chains and hence promoted their proximity and subsequent hydrogen bonding. Interestingly, our AX did not contain acidic monosaccharides, so the effect of ionic interactions in our hydrogels could be assumed as negligible. Moreover, our study showed that the same rheological changes happen not only at pH 2.0 but also at pH 5.0 and pH 7.0. Therefore, the mechanism resulting in higher moduli after regeneration seems to be related to further interactions within the hydrogel network. Hence, we hypothesize that the strong gel formation by regeneration of FAX-CL is likely due to the chain re-arrangement of polysaccharides during the freeze-drying step instead of ionic interactions, either backbone interactions between the unsubstituted junctions in the xylan backbone and/or larger-scale aggregative network interactions. Freeze-drying has been reported to lead to changes in the hydrogen bonding and crystallinity of polymers (Liu, Martinez-Sanz, Lopez-Sanchez, Gilbert, & Gidley, 2017; Ricciardi, Gaillet, Ducouret, Lafuma, & Lauprêtre, 2003). Although hemicelluloses are accepted as amorphous molecules (Werner, Pommer, & Broström, 2014), xylans can be semi-crystalline depending on the degree of substitution (Heikkinen et al., 2013; Hoije et al., 2008).

Therefore, we further investigated the morphology and multiscale structure of FAX-CL and its regenerated hydrogels to shed light on the effect of the possible crystallinity and other network interactions on the distinct gelation mechanisms leading to the formation of weak and strong FAX gels.

3.4. Multiscale structural characterization of FAX hydrogels

The microstructure of FAX-CL and its regenerated hydrogels (FAX-CL-pH2, FAX-CL-pH5 and FAX-CL-pH7) was analyzed by cryo-SEM after high pressure freezing. The cryo-SEM images and the porosity values of the hydrogels are presented in Fig. 4a–d and Table 3, respectively. FAX-CL exhibited a highly porous microstructure as a typical characteristic of polysaccharide gels. The regeneration, on the other hand, resulted in different porosity and pore sizes depending on the pH. FAX-CL-pH2 exhibited the most compact microstructure with the lowest porosity among the hydrogels. The porosity gradually increased as the regeneration pH was increased; however, it never reached the maximum porosity value of FAX-CL. This stiffer structure of the regenerated hydrogels could explain their higher mechanical strength. Furthermore, the lower porosity of the regenerated hydrogels may be attributed to the enhanced physical interactions between crosslinked AX clusters, which placed these domains closer. This can be attributed to the hindering effect of freeze drying on the mobility of the AX domains. As the regeneration pH increased, physical interactions became less efficient resulting from weaker protonation and led to higher porosity in FAX-CL-pH5 and FAX-CL-pH7.

To understand the mechanism behind the gelation of FAX and the differences between the native and regenerated hydrogels at different length scales, WAXS and SAXS measurements were performed and correlated with the microstructure observations. As the regenerated hydrogels exhibited similar rheological behavior, we decided to focus on the FAX-CL-pH2 hydrogel that exhibited the most distinct porous structure from the cryo-SEM measurements.

The crystalline behavior of the FAX solution and the hydrogels (FAX-CL and FAX-CL-pH2) was studied by WAXS as presented in Fig. 5a. The samples showed four common crystalline peaks with similar characteristic distances (d values) and a wide amorphous peak centered at $2\theta = 21°$, indicating that all samples were semi-crystalline. The scattering patterns were fitted to identify the center of the crystalline peak and to quantify the contribution of the amorphous and crystalline components (Fig. 5b–d and Table 2). The degree of crystallinity, X_c, of the samples was calculated using the ratio of the total area of crystalline peaks to the total area of the diffractograms (amorphous and crystalline contribution). The d values for the crystalline peaks were $d_1 = 0.83$ nm, $d_2 = 0.73$ nm, $d_3 = 0.48$ nm, $d_4 = 0.40$ nm and $d_5 = 0.36$ nm (Table 2) and these were in agreement with the results reported for xylan hydrate by Nieduszynski and Marchessault (1972). The WAXS patterns of the FAX solution showed significantly lower X_c value than that of the crosslinked samples (FAX-CL and FAX-CL-pH2) (Table 2). This suggested that enzymatic crosslinking leads to a higher level of organization at the molecular level of the AX chains, caused by the proximity between AX chains upon the formation of diferulic bridges and favored by the low degree of substitution of wheat bran AX. Interestingly, the regeneration induced a lower degree of crystallinity in FAX-CL-pH2 than that of FAX-CL. This could be explained by the different time scales of the enzymatic crosslinking reaction and the regeneration process. The enzymatic crosslinking of FAX is a process with slow kinetics (in the hour scale), whereas freezing and regeneration occur instantly with the rehydration of FAX-CL. The slower action of the enzymatic crosslinking might enable the reorganization of polymeric chains leading to a more ordered and crystalline structure, whereas regeneration prevents this re-organization and may even disrupt the available crystalline domains resulting in lower X_c values in FAX-CL-pH2.

The results of the WAXS measurement corroborate that enzymatic crosslinking increases the proximity of AX chains and thus results in a
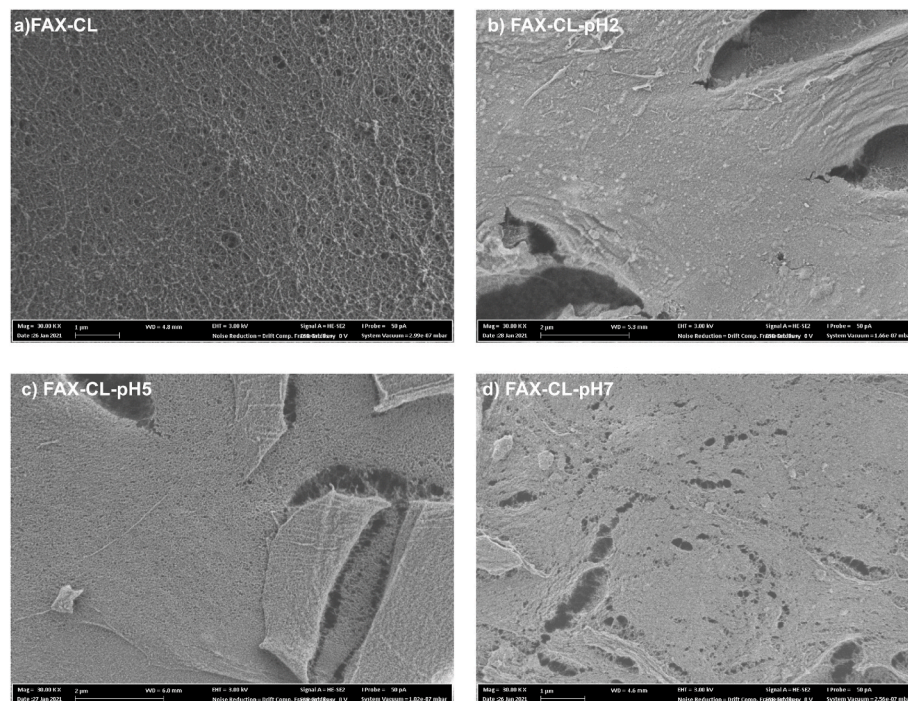
Fig. 4. Cryo-SEM images of (a) FAX-CL, (b) FAX-CL-pH2, (c) FAX-CL-pH5 and (d) FAX-CL-pH7.

Table 2
Degree of crystallinity (X_C) and d-spacing of native FAX solution and crosslinked FAX.

	X_C (%)	d_1 (nm)	d_2 (nm)	d_3 (nm)	d_4 (nm)	d_5 (nm)
FAX solution	15.9 ± 0.3[a]	0.83 ± 0.01	0.73 ± 0.02	0.48 ± 0.01	0.40 ± 0.01	0.36 ± 0.01
FAX-CL	28.3 ± 0.7[b]	0.84 ± 0.01	0.73 ± 0.01	0.48 ± 0.01	0.40 ± 0.01	0.36 ± 0.01
FAX-CL-pH2	23.1 ± 0.4[c]	0.84 ± 0.01	0.73 ± 0.01	0.48 ± 0.01	0.40 ± 0.01	0.36 ± 0.01

Superscript letters: *t*-test of 2 replicates (p < 0.05).

Table 3
Fitting parameters of the correlation length model of SAXS data from FAX crosslinked by laccase (FAX-CL) and regenerated at pH 2.0 (FAX-CL-pH2).

	Porosity (%)	n	m	ξ (nm)
FAX-CL	35.33	2.58 ± 0.05	3.1 ± 0.4	9.5 ± 0.8
FAX-CL-pH2	5.00	2.84 ± 0.09	2.7 ± 0.3	11.3 ± 0.11
FAX-CL-pH5	11.20	n.d.	n.d.	n.d.
FAX-CL-pH7	16.00	n.d.	n.d.	n.d.

n.d. Not determined.

more ordered and compact structure. The rise in X_c after crosslinking may further imply an increase in the secondary interactions (most likely hydrogen bonding) between adjacent AX chains. Considering the remarkable increase in the dynamic moduli of the regenerated hydrogels, these results indicate the existence of structural differences beyond the crystalline structure of these samples, i.e. at larger size scales (as discussed later in the SAXS results section).

The lattice parameters, *a, b* and *c* for FAX and FAX-CL unit cells were calculated assuming the same hexagonal crystalline structure reported by Heikkinen et al. (2013) for films from enzymatically tailored wheat endosperm AX (WAX-m). This model was chosen due to the similarities in the diffraction patterns and the DS (A/X: 0.29 in Heikkinen et al. (2013) and A/X: 0.23 in our case (Yilmaz-Turan, Jimenez-Quero, Menzel, et al., 2020) The chain axis of all the samples had the same

value as the xylan dihydrate (a = b = 0.963 nm). The lattice parameter *c* for FAX solution, FAX-CL and FAX-CL-pH2 was 1.49, 1.54 and 1.50 nm, respectively, as concurrent with the characteristics of xylan at 100% relative humidity (Nieduszynski & Marchessault, 1972). The slight increase in the lattice parameter *c* for FAX-CL and FAX-CL-pH2 showed that the volume of the unit cell somewhat increased by the crosslinking of AX. However, this increase did not have substantial implications in terms of the conformational changes of AX. Compared to the WAX-m sample from Heikkinen et al. (2013), FAX solution had a higher X_c, which could be purely due to the hydrated state of FAX solution as it is known to increase crystallinity (Kačuráková, Belton, Wilson, Hirsch, & Ebringerová, 1998).

To further understand the structural differences between the crosslinked and regenerated hydrogels at the nanoscale level, we performed SAXS measurements of FAX-CL and FAX-CL-pH2. The intensity data, *I(q)* was successfully fitted using the correlation length model as described by Equation (1) (Hammouda, Ho, & Kline, 2004; Yang et al., 2016):

$$I(q) = \frac{A}{q^n} + \frac{C}{1 + (q\xi)^m} + B \tag{1}$$

where *n* is the power-law exponent, *A* is the power-law coefficient, *m* is the Lorentz exponent, C is the Lorentz coefficient, ξ is the correlation length for the polymer chains and *B* is the background. The correlation length model was chosen as it describes the scattering of biphasic systems consisting of polymer chains and large size clusters (Hammouda et al., 2004), and the FAX hydrogel systems were composed of crosslinked AX clusters together with free polymeric chains. This model contains a first term describing the power-law scattering from clusters in the low q region and a second term, the Lorentzian term, describing scattering from polymer chains in the high *q* region. The correlation length, ξ, describes the mesh size of the gel in physical gels or the size of the growing aggregates in chemically crosslinked gels (Bode et al., 2013).

The fitting of the data and the parameters obtained from the model are presented in Fig. 5e and Table 3, respectively. The power-law exponents, *n*, was in the range of 1<*n* < 3, indicating that both hydrogels were mass fractals. The power-law exponent of FAX-CL-pH2 was higher
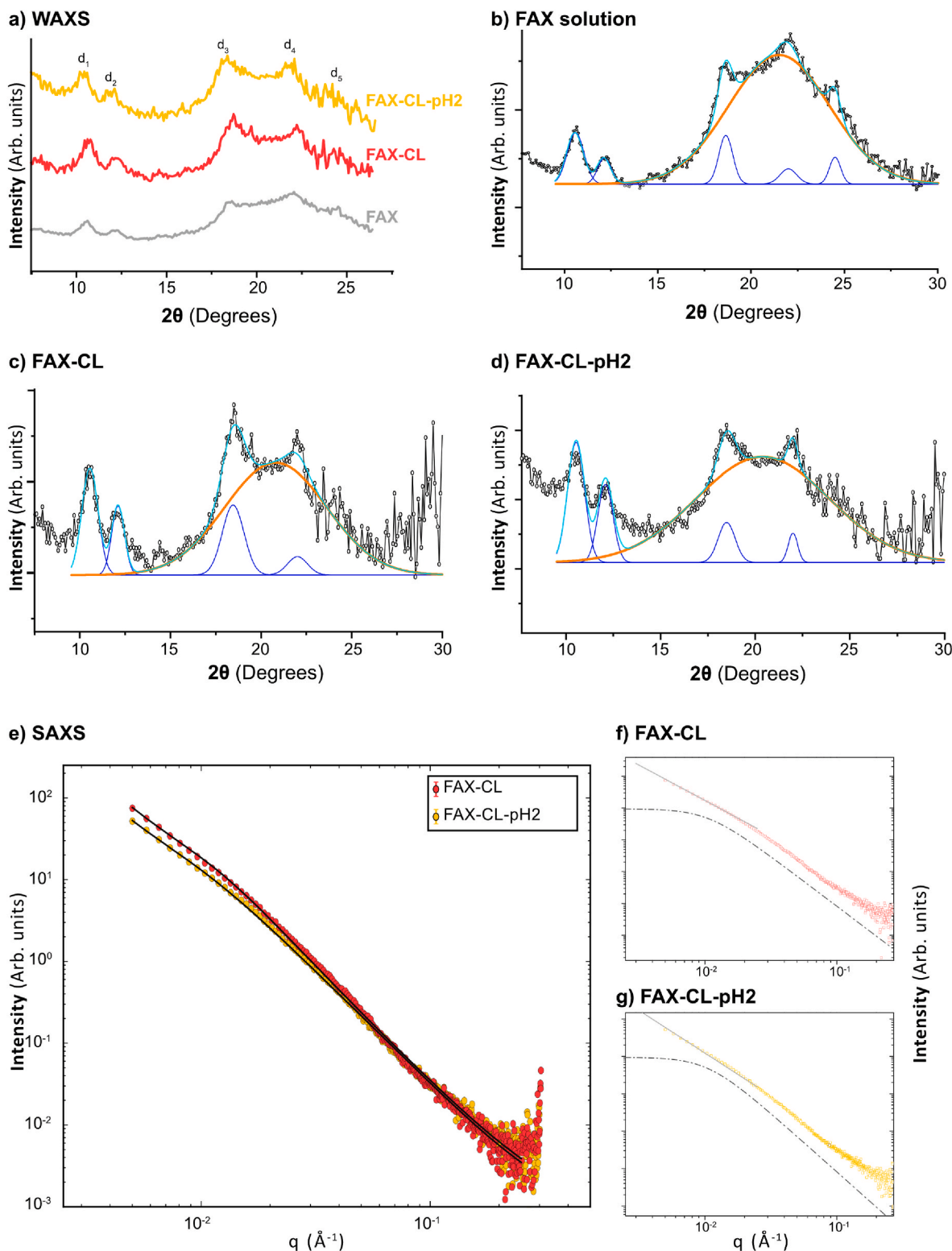
Fig. 5. Structural characterization of wheat bran arabinoxylan in solution (FAX), crosslinked (FAX-CL) and regenerated state (FAX-CL-pH2, FAX-CL-pH5 and FAX-CL-pH7). (a) WAXS curves of FAX solution, FAX-CL and FAX-CL-pH2; (b–d) Fittings of the diffractograms; (e) SAXS curves of FAX-CL and FAX-CL-pH2 together with fits; and (f–g) Scattering from FAX-CL and FAX-CL-pH2 showing the two components of the model; the Lorentzian (dashed line) and the power-law (solid line).

than that of FAX-CL, suggesting that the density of the crosslinked AX clusters in the former was higher. Furthermore, this was correlated with the lower porosity of FAX-CL-pH2 observed by cryo-SEM (Fig. 4). Seemingly, the higher cluster density of FAX-CL-pH2 resulted from the enhanced physical interactions between AX chains that increased their

proximity and resulted in a significantly less porous material. In the high-q regime, the Lorentz exponent m, can be related to the local chain conformations, with more expanded polymer chains typically having lower m values (Yang et al., 2016). The m value of FAX-CL was slightly higher than that of FAX-CL-pH2 however, the difference was inside the

experimental error. Therefore, we speculate that the compactness of the polymer chains of both FAX-CL and FAX-CL-pH2 was similar.

The local chain network can be further characterized by their correlation length, ξ. FAX-CL-pH2 had a higher ξ, implying that the size of the aggregates was larger in this hydrogel as a result of the regeneration step. The larger aggregate formation could be related to the fact that regeneration enhances hydrogen bonding. The differences between the fitting parameters of FAX-CL and FAX-CL-pH2 strongly suggest that auxiliary physical interactions occur between polysaccharide chains besides covalent crosslinking, when regeneration was employed. Among other parameters, the higher correlation length of FAX-CL-pH2 indicates that potential physical interactions, particularly hydrogen bonds, create tighter FAX domains resulting in larger aggregates. Furthermore, the presence of additional interactions in the FAX-CL-pH2 network may account for the substantially higher G' of this hydrogel. It appears from these results that the density of the crosslinked clusters is partially intensified by physical network formation during freeze drying and regeneration and this, in turn, improves the rheological performance of the regenerated hydrogels.

3.5. Model for the gelation mechanism and multiscale organization of FAX hydrogels

The quantity of FA units covalently attached to the AX chains has been postulated as the main parameter influencing the formation of hydrogels from FAX and their strength (Carvajal-Millan, Landillon, et al., 2005). While this is true, other structural parameters related to the non-covalent physical interactions between FAX chains and the network structure also play a significant role. In this direction, molecular properties such as the degree of Ara*f* substitution of FAX seems to be a critical factor influencing their gelation mechanism. Our study indeed suggests that the crosslinking of FAX with low Ara*f* substitution is different from highly substituted AX, being able to readily form gels by crosslinking in neutral conditions even with lower FA content (Carvajal-Millan, Guilbert, Morel, & Micard, 2005). In our study, wheat bran FAX contained a substantial amount of FA (7.49 mg/g AX) but was moderately substituted (A/X: 0.23), therefore they were not expected to form gels with high viscoelasticity. Interestingly, we observed a significant

increase in the degree of crystallinity of FAX after enzymatic crosslinking and important changes both in the rheological and structural properties at the nanoscale following the regeneration at pH 2.0. Based on these results we propose the following gelation mechanism for moderately substituted FAX at different pH conditions. We also present a scheme showing the structure of crosslinked and regenerated FAX in Fig. 6, based on the results of the WAXS and SAXS measurements.

Chemical crosslinking of FAX favors re-organization of the polymeric chains and the increase of intermolecular interactions, leading to more compact polymeric conformations and higher chain packing (e.g. higher X_c). A higher-ordered structure of the crosslinked FAX was also indicated by higher Mw and gel characteristics as shown in the SEC results and mechanical spectra, respectively. The AX chains can be expected to randomly form ordered structures due to the heterogeneous localization of the formed covalent crosslinks, which in the end results in the generation of polysaccharide networks with aggregates and clusters at the nanoscale. Upon freeze drying and regeneration, on the other hand, the physical interactions between FAX chains increase and the distance between the chains decreases. Hereby, the aggregates further grow and start interconnecting to a higher extent forming larger and denser clusters that possess remarkable viscoelastic properties. We hypothesize that the covalent crosslinks do not play a substantial role in this length scale. The results of our study demonstrated that regenerated FAX hydrogels can withstand a range of pH (between 2.0 and 7.0) without getting hydrolyzed/degraded. These pH-resistant characteristics of FAX hydrogels make them suitable for food and pharmaceutical applications in which acidic conditions are used during manufacturing or for control release of drugs and bioactive compounds in the gastrointestinal tract.

4. Conclusions

We have prepared hydrogels by enzymatic crosslinking via laccase oxidation of moderately substituted wheat bran feruloylated arabinoxylan (FAX) and further regeneration at different pH conditions. The conversion of monomeric ferulic acid into five different forms of ferulic acid dimers verified that the laccase enzyme was efficient to oxidize the available ferulic acid units during oxidative coupling. The enzymatic crosslinking changed the conformation of native FAX into a more
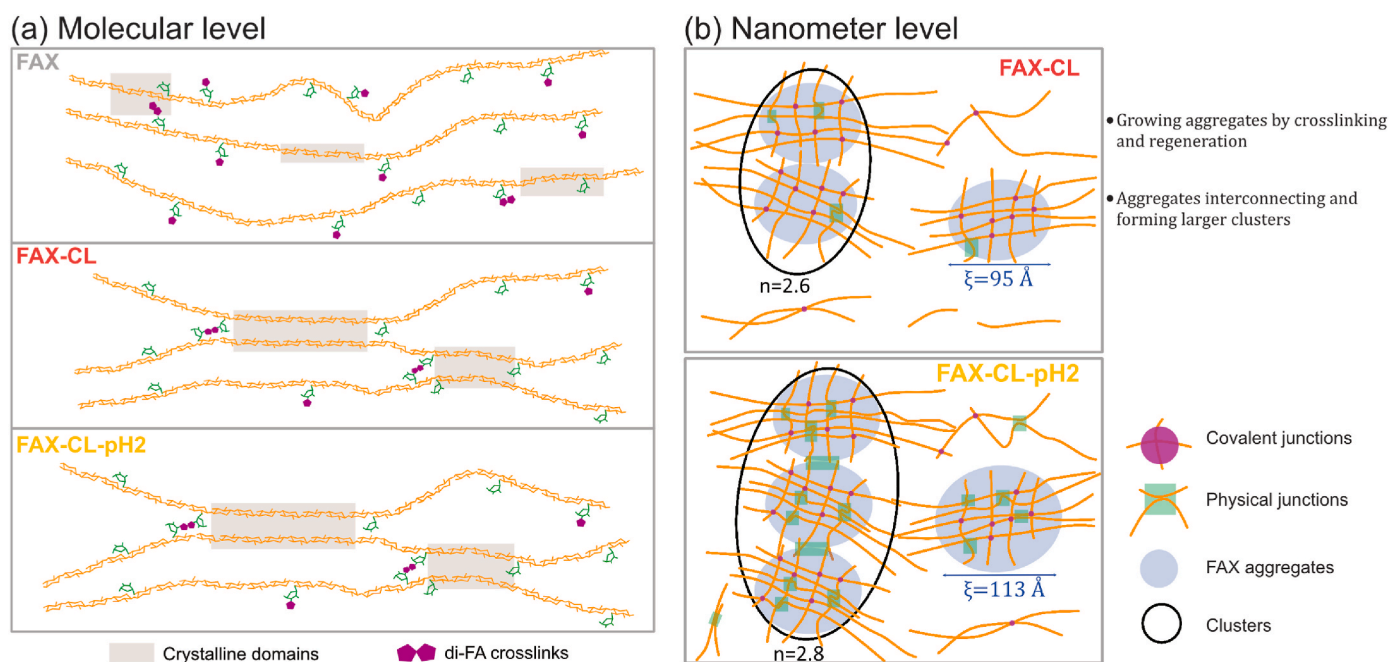

Fig. 6. Model representing the multiscale structure of native, crosslinked and regenerated FAX. a) Molecular organization of FAX, FAX-CL and FAX-CL-pH2, and b) Nanoscale organization of FAX-CL and FAX-CL-pH2.

ordered and tightly packed structure with higher degree of crystallinity while increasing the molecular weight. The regeneration approach remarkably increased the viscosity and dynamic moduli of FAX regardless of the pH, resulting in stronger hydrogels. The rheological measurements demonstrated that the mechanical behavior of the FAX hydrogels can be tuned by chemical (crosslinking) and physical (regeneration) effects. The semicrystalline characteristics of the structure of the FAX solution was enhanced by the crosslinking while the regeneration step decreased the crystallinity due to physical effects. Combining with the nanostructure, the findings of this study revealed the role of physical interactions in the formation of FAX hydrogels in addition to covalent crosslinks since the regeneration increases the size of the aggregates (ξ) formed in the crosslinking and forms denser clusters at a higher level.

Overall, the hydrogels produced from moderately substituted FAX demonstrated high mechanical strength while maintaining their structural integrity. Bearing in mind that the feruloylation confers wheat bran AX with additional functionalities, such as antioxidant capacity, the hereby studied hydrogels may find application in food and biomedical products where pH stability and preservation against oxidation are required.

Author statement

Secil Yilmaz Turan: Conceptualization, Investigation, Formal analysis, Methodology, Data curation, Visualization, Writing – original draft, Writing – review & editing. **Patricia Lopez-Sanchez:** Investigation, Formal analysis, Methodology, Writing – review & editing. **Amparo Jiménez-Quero:** Investigation, Supervision, Writing – review & editing. **Tomás S. Plivelic:** Investigation, Formal analysis, Methodology, Writing – review & editing. **Francisco Vilaplana:** Conceptualization, Supervision, Writing – review & editing, Project administration, Funding acquisition.

Declaration of competing interest

The authors declare that they have no known competing financial interests or personal relationships that could have appeared to influence the work reported in this paper.

Acknowledgments

Appendix A. Supplementary data

Supplementary data to this article can be found online at https://doi.org/10.1016/j.foodhyd.2022.107575.

References

Bode, F., da Silva, M. A., Smith, P., Lorenz, C. D., McCullen, S., Stevens, M. M., et al. (2013). Hybrid processes in enzymatically gelled gelatin: Impact on , macroscopic properties and cellular response. *Soft Matter, 9*(29), 6986–6999.

Borjesson, M., Westman, G., Larsson, A., & Strom, A. (2019). Thermoplastic and flexible films from arabinoxylan. *ACS Appl. Polym. Mater., 1*(6), 1443–1450.

Carvajal-Millan, E., Guilbert, S., Morel, M. H., & Micard, V. (2005a). Impact of the structure of arabinoxylan gels on their rheological and protein transport properties. *Carbohydrate Polymers, 60*(4), 431–438.

Carvajal-Millan, E., Landillon, V., Morel, M. H., Rouau, X., Doublier, J. L., & Micard, V. (2005b). Arabinoxylan gels: Impact of the feruloylation degree on their structure and properties. *Biomacromolecules, 6*(1), 309–317.

Hammouda, B., Ho, D. L., & Kline, S. (2004). Insight into clustering in poly(ethylene oxide) solutions. *Macromolecules, 37*(18), 6932–6937.

Heikkinen, S. L., Mikkonen, K. S., Pirkkalainen, K., Serimaa, R., Joly, C., & Tenkanen, M. (2013). Specific enzymatic tailoring of wheat arabinoxylan reveals the role of substitution on xylan film properties. *Carbohydrate Polymers, 92*(1), 733–740.

Hoije, A., Sternemalm, E., Heikkinen, S., Tenkanen, M., & Gatenholm, P. (2008). Material properties of films from enzymatically tailored arabinoxylans. *Biomacromolecules, 9* (7), 2042–2047.

Kačuráková, M., Belton, P. S., Wilson, R. H., Hirsch, J., & Ebringerová, A. (1998). Hydration properties of xylan-type structures: An FTIR study of xylooligosaccharides. *Journal of the Science of Food and Agriculture, 77*(1), 38–44.

Kaur, A., Yadav, M. P., Singh, B., Bhinder, S., Simon, S., & Singh, N. (2019). Isolation and characterization of arabinoxylans from wheat bran and study of their contribution to wheat flour dough rheology. *Carbohydrate Polymers, 221*, 166–173.

Khalighi, S., Berger, R. G., & Ersoy, F. (2019). Cross-linking of wheat bran arabinoxylan by fungal laccases yields firm gels. *Processes, 8*(1).

Liu, D., Martinez-Sanz, M., Lopez-Sanchez, P., Gilbert, E. P., & Gidley, M. J. (2017). Adsorption behaviour of polyphenols on cellulose is affected by processing history. *Food Hydrocolloids, 63*, 496–507.

Marquez-Escalante, J. A., Carvajal-Millan, E., Yadav, M. P., Kale, M., Rascon-Chu, A., Gardea, A. A., et al. (2018). Rheology and microstructure of gels based on wheat arabinoxylans enzymatically modified in arabinose to xylose ratio. *Journal of the Science of Food and Agriculture, 98*(3), 914–922.

Martinez-Lopez, A. L., Carvajal-Millan, E., Marquez-Escalante, J., Campa-Mada, A. C., Rascon-Chu, A., Lopez-Franco, Y. L., et al. (2019). Enzymatic cross-linking of ferulated arabinoxylan: Effect of laccase or peroxidase catalysis on the gel characteristics. *Food Sci. Biotechnol., 28*(2), 311–318.

Mathew, S., Abraham, T. E., & Zakaria, Z. A. (2015). Reactivity of phenolic compounds towards free radicals under in vitro conditions. *Journal of Food Science & Technology, 52*(9), 5790–5798.

Mendis, M., & Simsek, S. (2014). Arabinoxylans and human health. *Food Hydrocolloids, 42*(Part 2), 239–243.

Menzel, C., Gonzalez-Martinez, C., Chiralt, A., & Vilaplana, F. (2019). Antioxidant starch films containing sunflower hull extracts. *Carbohydrate Polymers, 214*, 142–151.

Nieduszynski, I. A., & Marchessault, R. H. (1972). Structure of β,D(1–>4′)-xylan hydrate. *Biopolymers, 11*(7), 1335–1344.

Prückler, M., Siebenhandl-Ehn, S., Apprich, S., Höltinger, S., Haas, C., Schmid, E., et al. (2014). Wheat bran-based biorefinery 1: Composition of wheat bran and strategies of functionalization. *Lebensmittel-Wissenschaft und -Technologie- Food Science and Technology, 56*(2), 211–221.

Ricciardi, R., Gaillet, C., Ducouret, G., Lafuma, F., & Lauprêtre, F. (2003). Investigation of the relationships between the chain organization and rheological properties of atactic poly(vinyl alcohol) hydrogels. *Polymer, 44*(11), 3375–3380.

Rigaku Innovative Technologies, I., & XRay-Sytems-ApS, J. J.- (2010). *SAXSGUI User's Guide (v2.05.02). A graphical user interface for visualizing, transforming and reducing SAXS images* (as well as limited fitting).

Rosicka-Kaczmarek, J., Komisarczyk, A., Nebesny, E., & Makowski, B. (2016). The influence of arabinoxylans on the quality of grain industry products. *European Food Research and Technology, 242*(3), 295–303.

Ruthes, A. C., Martínez-Abad, A., Tan, H.-T., Bulone, V., & Vilaplana, F. (2017). Sequential fractionation of feruloylated hemicelluloses and oligosaccharides from wheat bran using subcritical water and xylanolytic enzymes. *Green Chemistry, 19*(8), 1919–1931.

Ruthes, A. C., Rudjito, R. C., Rencoret, J., Gutiérrez, A., del Río, J. C., Jiménez-Quero, A., et al. (2020). Comparative recalcitrance and extractability of cell wall polysaccharides from cereal (wheat, rye, and barley) brans using subcritical water. *ACS Sustainable Chemistry & Engineering, 8*(18), 7192–7204.

SasView. http://www.sasview.org/.

Schuster, E., Cucheval, A., Lundin, L., & Williams, M. A. (2011). Using SAXS to reveal the degree of bundling in the polysaccharide junction zones of microrheologically distinct pectin gels. *Biomacromolecules, 12*(7), 2583–2590.

Stevanic, J. S., Joly, C., Mikkonen, K. S., Pirkkalainen, K., Serimaa, R., Remond, C., et al. (2011). Bacterial nanocellulose-reinforced arabinoxylan films. *Journal of Applied Polymer Science, 122*(2), 1030–1039.

Vansteenkiste, E., Babot, C., Rouau, X., & Micard, V. (2004). Oxidative gelation of feruloylated arabinoxylan as affected by protein. Influence on protein enzymatic hydrolysis. *Food Hydrocolloids, 18*(4), 557–564.

Vilaplana, F., & Gilbert, R. G. (2010). Two-dimensional size/branch length distributions of a branched polymer. *Macromolecules, 43*(17), 7321–7329.

Vismeh, R., Lu, F., Chundawat, S. P., Humpula, J. F., Azarpira, A., Balan, V., et al. (2013). Profiling of diferulates (plant cell wall cross-linkers) using ultrahigh-performance liquid chromatography-tandem mass spectrometry. *Analyst, 138*(21), 6683–6692.

Werner, K., Pommer, L., & Broström, M. (2014). Thermal decomposition of hemicelluloses. *Journal of Analytical and Applied Pyrolysis, 110*(Supplement C), 130–137.

Yang, Z., Hemar, Y., Hilliou, L., Gilbert, E. P., McGillivray, D. J., Williams, M. A., et al. (2016). Nonlinear behavior of gelatin networks reveals a hierarchical structure. *Biomacromolecules, 17*(2), 590–600.

Yilmaz-Turan, S., Jimenez-Quero, A., Menzel, C., de Carvalho, D. M., Lindstrom, M. E., Sevastyanova, O., et al. (2020a). Bio-based films from wheat bran feruloylated arabinoxylan: Effect of extraction technique, acetylation and feruloylation. *Carbohydrate Polymers, 250*, 116916.

Yilmaz-Turan, S., Jimenez-Quero, A., Moriana, R., Arte, E., Katina, K., & Vilaplana, F. (2020b). Cascade extraction of proteins and feruloylated arabinoxylans from wheat bran. *Food Chemistry, 333*, 127491.

Yu, L., Yakubov, G. E., Gilbert, E. P., Sewell, K., van de Meene, A. M. L., & Stokes, J. R. (2019). Multi-scale assembly of hydrogels formed by highly branched arabinoxylans from Plantago ovata seed mucilage studied by USANS/SANS and rheology. *Carbohydrate Polymers, 207*, 333–342.

Zhang, X., Chen, T., Lim, J., Gu, F., Fang, F., Cheng, L., et al. (2019). Acid gelation of soluble laccase-crosslinked corn bran arabinoxylan and possible gel formation mechanism. *Food Hydrocolloids, 92*, 1–9.

Zhang, Y., Pitkanen, L., Douglade, J., Tenkanen, M., Remond, C., & Joly, C. (2011). Wheat bran arabinoxylans: Chemical structure and film properties of three isolated fractions. *Carbohydrate Polymers, 86*(2), 852–859.